Small-Size Tapered Slot Antenna (TSA) Design for use in 5G Phased Array Applications

Naser Ojaroudi Parchin, Ming Shen, and Gert Frølund Pedersen

Antennas, Propagation, and Radio Networking (APNet) Section
Department of Electronic Systems, Faculty of Engineering and Science
Aalborg University, DK-9220, Aalborg, Denmark
naser@es.aau.dk, mish@es.aau.dk, gfp@es.aau.dk

Abstract ─ The design and development of a compact tapered slot antenna (TSA) for the fifth generation (5G) phased array communications is described in this manuscript. The proposed low-profile TSA element is designed on a *Rogers RT 5880* (ε=2.2 and δ=0.0009) dielectric to work in the frequency range from 21 to 23 GHz. The configuration of the employed TSA antenna elements is composed of a slot-line flare from a small gap to a large opening, matching to free space's wave impedance. Eight TSA elements with well-defined end-fire radiation patterns have been used on the top portion of a mobile-phone PCB to form a 1×8 linear phased array. The TSA elements are fed by hockey-stick baluns. In addition, the radiation performance and SAR characteristics of the phased array 5G antenna in the vicinity of user's hand & head have been investigated in this study. The results show that the proposed design provides good characteristics in terms of S-parameters, antenna gain, efficiency, SAR, and beam steering, which fit the need of 5G cellular communications.

Index Terms ─ 5G wireless networks, cellular communications, planar phased array, TSA.

I. INTRODUCTION

The fifth generation (5G) networks are expected to use the higher frequency bandwidths due to the growing need for wider bandwidths and higher data rates [1-2]. Compared with the cellular networks used today (operating at the frequencies less than 4 GHz), 5G mobile networks will use broader mm-Wave frequency bandwidths [3]. 22 GHz, 28 GHz, and 38 GHz are some of the candidate bands for 5G wireless communications [4-5]. Different from the conventional antennas (patch and slot antennas) in order to cover the required coverage-space of 5G communications, the end-fire antennas, such as horn waveguide antenna, Yagi antenna and linear tapered slot antenna (LTSA) are more suitable. Among them, the TSA is a promising candidate for reasons such as easy fabrication and easy integration [6-7]. Our work presents the study on the design of a

22 GHz phased array tapered slot antenna for the future 5G cellular communication applications.

Tapered slot antenna (TSA) has received considerable amount of research effort owing to their attractive futures such as high gain and relatively wide bandwidth compared with other designs such as typical patch antennas. They can provide excellent directional propagation at the higher frequencies and could be used for radar, detecting and phased array applications [8-9]. The TSA array with compact size and high-gain characteristics is also among one of the most promising candidates meeting the requirements of 5G systems, and hence, could be used to form multiple antenna systems for 5G systems [10].

The designed TSA element is operating from 21 to 23 GHz and has compact-size, sufficient-gain, high-efficiency, high-fidelity, and good end-fire radiation pattern. The designed antenna element has a good potential to be used in linear and planar phased array applications. Eight elements of the TSAs have been used to form a linear phased array in the edge region (top-side) of a 5G mobile phone PCB. Another set of the linear phased array could be used on the bottom portion of the PCB. The designed 5G phased array mobile-phone antenna provides good features in terms of fundamental radiation properties. Furthermore, 64-elements of the antennas are employed to form a planar phased array with high-gain property. More than 20 dB gain, and -0.5 dB (90%) total efficiency have been obtained when its beam is tilted to 0° elevation. The results show that the designed TSA arrays (linear & planar) satisfy general requirements for use in 5G platforms.

II. SINGLE ELEMENT TSA

The configuration of the single element TSA is shown in Fig. 1. As illustrated, it contains a slot-line flare from a small gap to a large opening, matching to free space's wave with hockey-stick balun feed technique. The strip-line/slot-line transition is specified by W_f (strip-line width) and W_2 (slot-line width). The

exponential taper profile is defined by the opening rate and two points P_1 (z_1, y_1) and P_2 (z_2, y_2):

$$y = c_1 e^{Rz} + c_2, \qquad (1)$$

where $c_1 = \dfrac{y_2 - y_1}{e^{Rz_2} - e^{Rz_1}}$ and $c_2 = \dfrac{y_1 e^{Rz_2} - y_2 e^{Rz_1}}{e^{Rz_2} - e^{Rz_1}}$.

The taper length L is z_2-z_1 and the aperture height H is $2(y_2-y_1)+W_f$. In the case where x approaches zero, the exponential taper results in a so-called linearly tapered slot antenna (LTSA) for which the taper slope is constant and given by $s_0= (y_2$-$y_1)/(z_2$-$z_1)$. For the exponential taper defined by (1), the taper slope changes continuously from s_1 to s_2, where s_1 and s_2 are the taper slope at $z=z_1$ and at $z=z_2$, respectively, and $s_1< s <s_2$ for $x>0$. The taper flare angle has been defined by $\alpha=tan^{-1}s$. In theory, the maximum opening width [11] is:

$$\lambda_g = \frac{c}{f_{min} \sqrt{\varepsilon_r}}, \qquad (2)$$

where C is speed of light, f_{min} is frequency minimum, and ε_r is dielectric constant of the substrate.
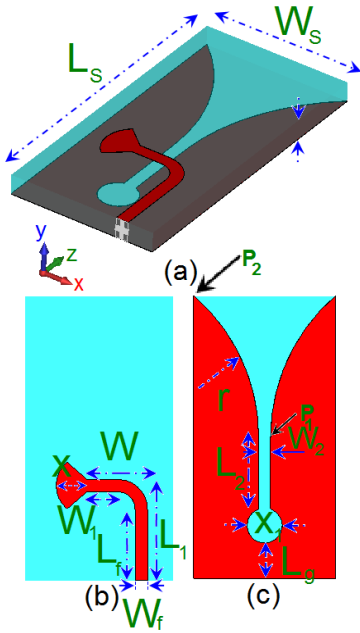

Fig. 1. Proposed TSA configuration: (a) side view, (b) top layer, and (c) bottom layer.

The equivalent circuit for the TSA is shown in Fig. 2. The total impedance Z_{RP} at the reference plane T on the strip-line can be expressed as a series connection of the strip-line stub reactance JX_{STB} and the antenna impedance Z_A [12]. Based on Fig. 2, Z_{input}(s) and $\Gamma_z(s)$ of the TSA can be calculated as:

$$Z_{input}(s) = L_1 S + R \| L_2 \| \frac{1}{C_1 S},$$

which is equal to:

$$Z_{input}(s) = S\left\{ \frac{(R_1 L_2 + R_1 L_1) + L_1 L_2 S + R_1 L_1 L_2 C S^2}{R_1 + L_2 S + R_1 L_2 C S_2} \right\}, \qquad (3)$$

$$\Gamma_z(s) = \frac{Z_{input}(s)}{Z_{input}(s) + 2Z_0}. \qquad (4)$$

The antenna has a compact size of $W_S \times L_S$. The design parameters of the antenna and the proposed array are specified in Table 1. The simulated S_{11} characteristic of the designed TSA is illustrated in Fig. 3. It can be seen that the proposed TSA antenna covers the frequency band from 21 to 23 GHz (2 GHz bandwidth for S_{11} less than -10) and has a reflection coefficient of -30 dB at the resonance frequency (22 GHz).
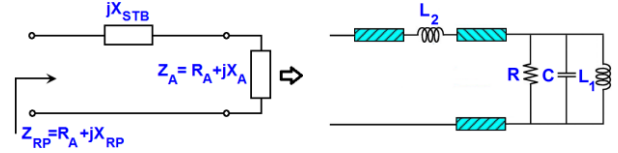

Fig. 2. Equivalent circuit for the TSA.

Table 1: Dimension of the antenna parameters

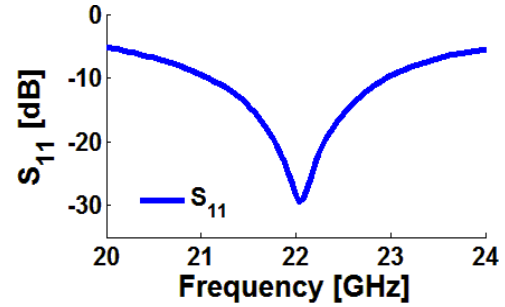| Parameter	W_X	L_X	W_S	$L_S=L_a$	W_a	h
Value (mm)	48	42.8	6	12	48	0.8
Parameter	L_g	W	L	W_1	L_1	r
Value (mm)	1.5	2.25	4	1.1	4.25	8
Parameter	W_2	L_2	W_f	L_f	X	X_1
Value (mm)	0.5	3	0.5	3	1.25	1.5

Fig. 3. S_{11} characteristic of the LTSA.

The frequency response (S_{11}) of the designed TSA can be controlled by changing the values of critical parameters such as the width of the hockey-stick balun. Figure 4 depicts the S_{11} characteristics of the antenna for different values of W_1. As illustrated, when the value of W_1 increases from 2.05 to 2.45 mm, the resonance of the antenna response increases from 22.05 to 22.6 GHz. The efficiency characteristics of the antenna over the operation band is described in Fig. 5 (a). In theory, the radiation and total efficienies are related according as:

$$e_0 = e_r e_{cd}. \qquad (5)$$

In addition, the 3D radiation pattern of the antenna at 22 GHz is illustrated in Fig. 5 (b). The antenna gain can be calculated using the total efficiency and the directivity as follows:

$$G_0 \, (dB) = 10 \log (e_0 D_0), \qquad (6)$$

where e_0 is the total antenna efficiency, er is reflection (mismatch) efficiency=$(1-|\Gamma|2)$, e_{cd} is antenna radiation efficiency and D_0 is the antenna directivity [13]. As can be seen, the antenna has a desirable end-fire radiation property with 4.45 dB gain (IEEE gain×missmatch). Based on the obtained results, the antenna has high efficiency function at the different frequency of the operation band (especially at the resonance frequency= 22 GHz).
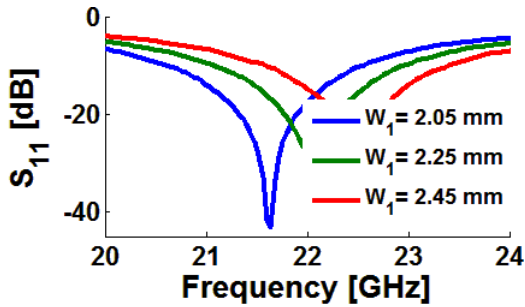
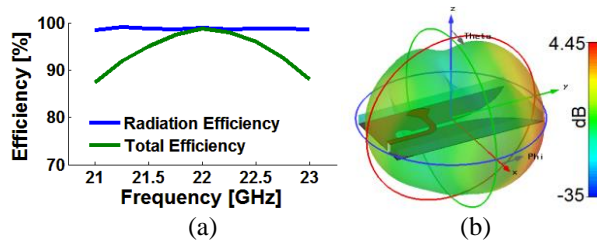Fig. 4. S_{11} curves for different values of W_1.

Fig. 5. Simulated (a) efficiencies and (b) radiation pattern of the designed TSA.

In the analysis on the microstrip antennas, the transfer function is transformed to time domain by performing the inverse Fourier transform. The fourth derivative of a Gaussian function is selected as the transmitted pulse. Therefore the output waveform at the receiving antenna terminal can be expressed by convoluting the input signal and the transfer function. The shape of the transmitted signal in free space is shown in Fig. 6.

The input and received waveforms for the face-to-face and side-by-side orientations of the antenna are shown in Fig. 7. It can be seen that the shape of the pulse is preserved in all the cases. There is slight distortion on received pulses but it was expected. Using the reference and received signals, it becomes possible to quantify the level of similarity between signals.
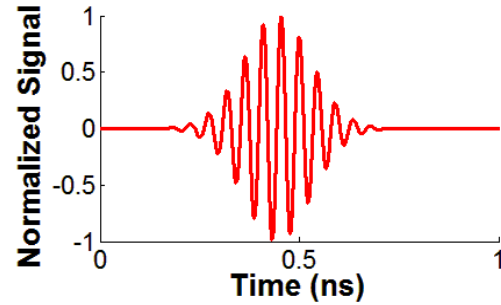

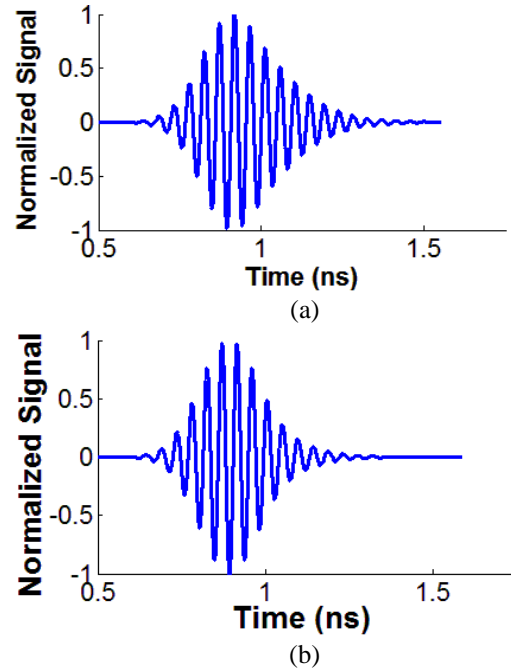Fig. 6. Transmitted signal in free space.

(a)

(b)

Fig. 7. Received pulses (a) side by side and (b) face to face.

In telecommunication systems, the correlation between the transmitted (T_X) and received (R_X) signals is evaluated using the fidelity factor (7):

$$F = Max_\tau \left| \frac{\int_{-\infty}^{+\infty} s(t)r(t-\tau)}{\sqrt{\int_{-\infty}^{+\infty} s(t)^2 \, dt . \int_{-\infty}^{+\infty} r(t)^2 \, dt}} \right|, \qquad (7)$$

where $s(t)$ and $r(t)$ are the T_X and R_X signals, respectively. For impulse radio in UWB communications, it is necessary to have a high degree of correlation between the TX and RX signals to avoid losing the modulated information. However for most of other telecommunication systems, the fidelity parameter is not that relevant. In order to evaluate the pulse transmission characteristics of the proposed antenna, two configurations (side-by-side and face-to-face

orientations) were chosen. The transmitting and receiving antennas were placed in a distance of $d=100$ mm. As shown in Fig. 7, although the received pulses in each of two orientations are broadened, a relatively good similarity exists between the R_X and T_X pulses. Using (7), the fidelity factor for the face-to-face and side-by-side configurations were obtained equal to 0.93 and 0.97, respectively. The obtained values of the fidelity factor show that the antenna imposes negligible effects on the transmitted pulses. The pulse transmission results are obtained using CST [14].

III. THE TSA LINEAR PHASED ARRAY

The proposed phased array antenna is designed using eight elements of TSAs. Figure 8 illustrates the configuration of the linear phased array. The array has a compact size of $W_a \times L_a = 48 \times 12$ mm^2. The antenna element are arranged with a distance of $d=W_S$.

Figure 9 shows the S parameters (S_{21} to S_{81}) of the array. As shown, the array has a good performance in the frequency range of 21 to 23 GHz. The highest mutual-coupling characteristic (S_{21}) between the TSA elements is less than -12 dB at the center frequency of the operation band (22 GHz).
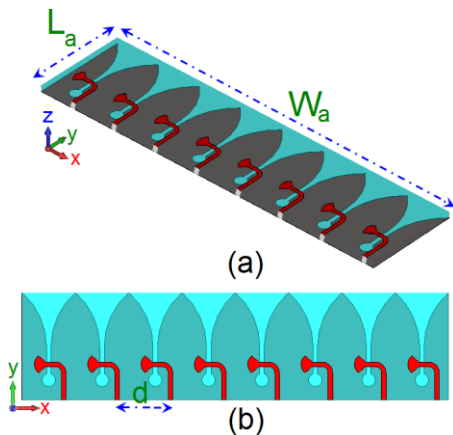

Fig. 8. Geometry of the linear array: (a) side view and (b) top view.
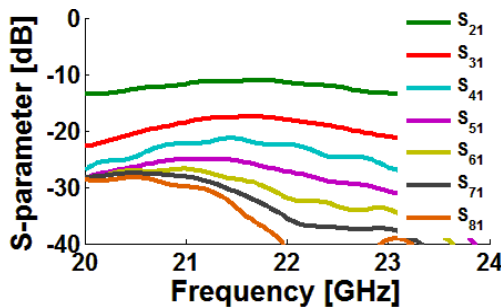

Fig. 9. S parameters of the array shown in Fig. 8.

In array designing, the adjacent element spacing must be chosen carefully due to its effect on the radiation performance of the array [15-16]. Figure 10 shows the configurations of the proposed array with different distance (d) between the elements. Simulated mutual coupling characteristics of the middle elements of the array for different values of d are illustrated in Fig. 11. As seen, in order to obtain a low mutual coupling characteristic for the antenna array, the distance between antenna elements must be near $\lambda/2$. When the distance between antenna elements increases from 7 to 5 mm, the mutual coupling characteristic of the array decreases from -9 to -16 dB. In addition, the radiation performance of the array for different values of d has been investigated.
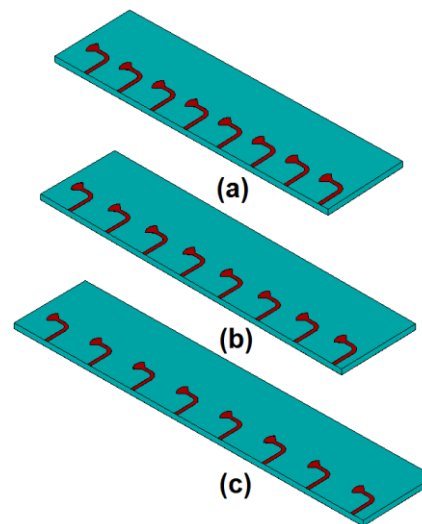

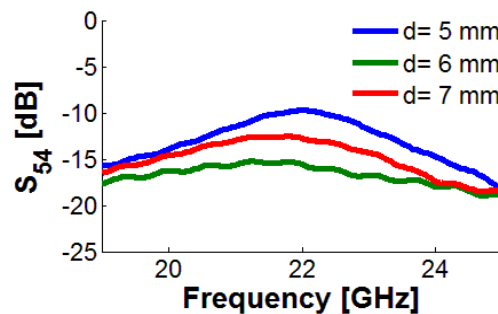Fig. 10. Side views of the array for: (a) d=5 mm, (b) d=6 mm, and (c) d=7 mm.

Fig. 11. Simulated S_{21} characteristics of the antenna for different values of d.

Figure 12 shows the main radiation beams of the array at 0° of scanning for different values of d. It can be seen for d=6 mm, the array has good efficiency, sufficienct gain level and compact size which is suitable

for cellular phased array applications. As illustrated, the array has 11.2, 12.2, and 12.7 dB gains with -0.54, -0.67, and -0.84 values of total efficiency for d=5 mm, d=6 mm, and d=7 mm, respectively. Based on the obtained results, in order to have high-gain, high-efficiency beams of antenna array with wide scanning function (0 to 75 degree), the distance between elements (*d*) must be calculated near $\lambda/2$ of the operation frequency (d=6 mm).
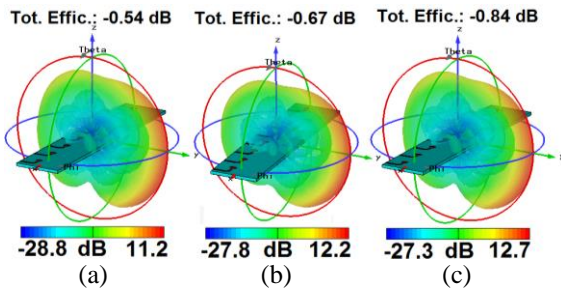

Fig. 12. 3D beams (at 0°) of the array for different values of *d*: (a) d=5 mm, (b) d=6 mm, and (c) d=7 mm.

Figure 13 (a) illustrates a system architecture in which the proposed linear phased array antenna can be used for 5G applications. For operations using time division duplex, the feed network can be implemented using low loss phase shifters (such as *HMC933LP4E* [17]) for beam steering). One of the important issues to achieve a functional array antenna is the feed network.
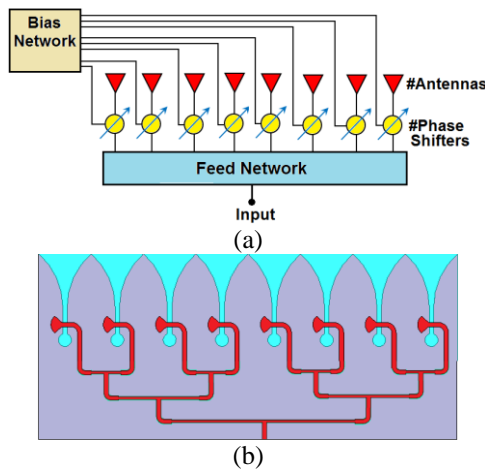

Fig. 13. (a) Phased array architecture for the proposed design, and (b) typical 1:8 feed network.

In the proposed design, a 1×8 uniform linear array antennas could be used and each radiating element with equal magnitude must be excited. There are various techniques of feed network design for this purpose: parallel [Fig. 13 (b)], series, and etc. The power dividers

(such as Wilkinson) divide the power to equally 1:N and also unequally by changing the input and output [9]. It should be noted the usage of the feed network could has influence on the antenna parameters in terms of directivity, mutual coupling, gain and etc. Additionally, the mutual coupling in combination with the feed network causes notable changes in the excitation currents. So, the losses of the antenna performance in the vicinity of feeding network and active elements should be considered.

IV. APPLICATION OF THE LINEAR ARRAY FOR 5G HANDHELD DEVICES

Figure 14 depicts the configuration of the 5G mobile-phone antenna. It consists of eight 22-GHz TSA elements used to form a linear phased array in the edge region (top-side) on a mobile phone PCB. Another set of the designed array could be used in two sets of phased arrays in the top and bottom portion of the mobile phone PCB [18].
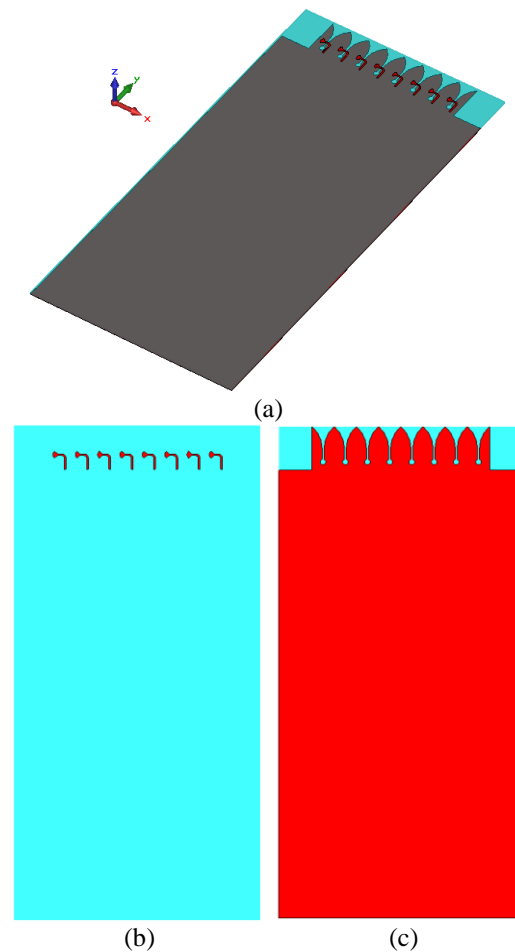

Fig. 14. Phased array 5G antenna configuration: (a) side view, (b) top layer, and (c) bottom layer (GND).

The simulated S-parameters (S_{11} to S_{81}) of the designed 5G mobile-phone antenna are shown in Fig. 15. The antenna operates at the central frequency of 22 GHz (2 GHz bandwidth). It can be seen that the highest mutual-coupling characteristic between the elements is less than -12 dB which is sufficient for typical phased array applications.
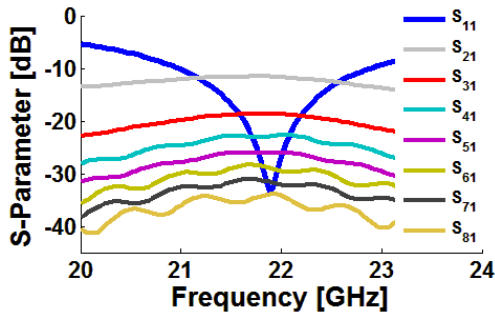

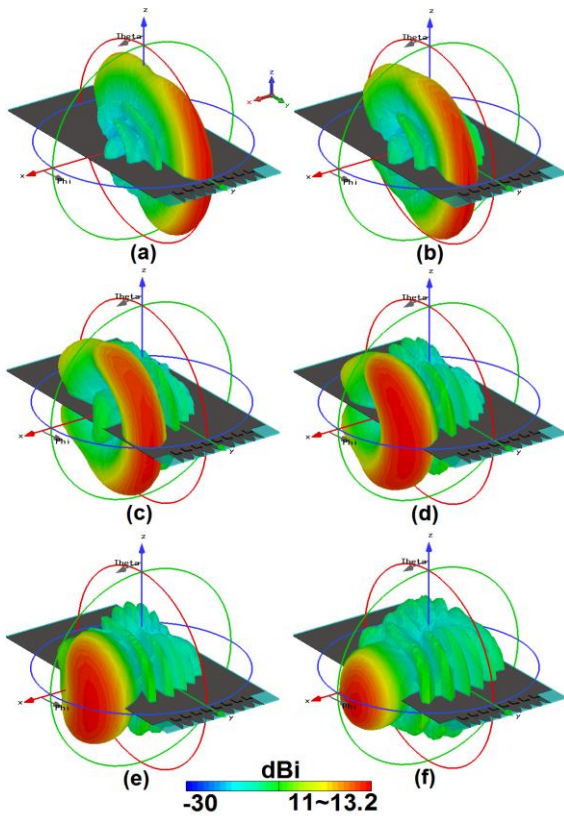Fig. 15. Simulated S-parameters of the proposed 5G mobile-phone antenna.

Fig. 16. 3D Radiation beams with directivity values at: (a) 0°, (b) 15°, (c) 30°, (d) 45°, (e) 60°, and (f) 75°.

The beam steering characteristic of the antenna with directivity values at different scanning angles

(0° to 75°) are shown in Fig. 16. The analysis and performance of the antenna beams are obtained by using CST Microwave Studio®. The shape and direction of the array beams are determined by relative phases amplitudes applied to each radiating element as below:

$$\psi = 2\pi (d / \lambda) \sin\theta, \qquad (8)$$

where d is the distance between the radiation elements and θ is the angle of incidence.

As seen, the proposed antenna has a sufficient beam-steering function in the scanning range of 0 to 75 degree. It should be noted that for plus-minus (±) scanning angles, the beam-steering characteristic of the antenna are almost the same. Figure 17 (a) illustrates the simulated realized gains of the proposed 5G mobile-phone antenna at different angles. From the beam steering characteristic, it can be observed that the antenna has sufficient gains at different scanning angles. For the scanning range of 0 to 75 degree, the antenna gains are almost constant and more than 10 dB.

Figure 17 (b) describes the fundamental radiation properties of the antenna beams for the scanning range of 0 to 70 degree. As seen, in the scanning angle of 0-60 degree, the antenna has more than -0.1 dB -0.5 dB radiation and total efficiencies, respectively. It is noted that the antenna has high efficiencies for different scanning angles. Furthermore, when the scanning angle of the radiation beam is ≤+60°, the proposed antenna has more than 11 dBi directivity.
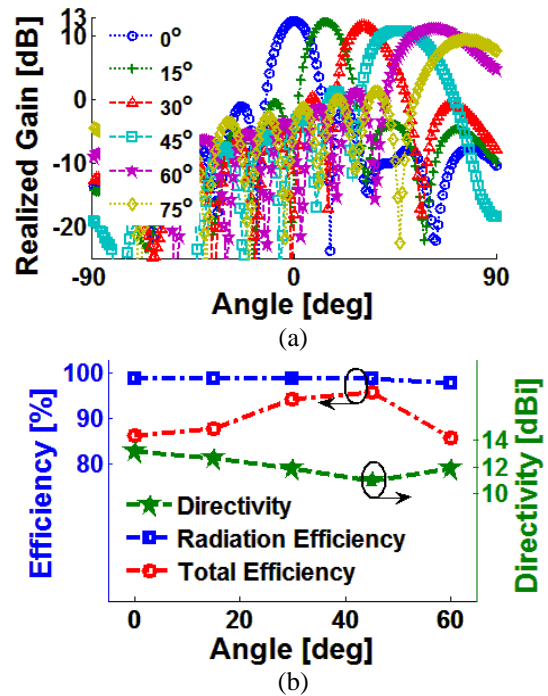

Fig. 17. (a) Realized gains and (b) radiation properties of the antenna at different scanning angles.

The radiation performances of the proposed 5G mobile-phone antenna with different lengths of the PCB ground-plane have been investigated in Fig. 18. As illustrated, the size of PCB ground plane does not have significant impact on the radiation properties of the antenna in terms of gain and total efficiency.
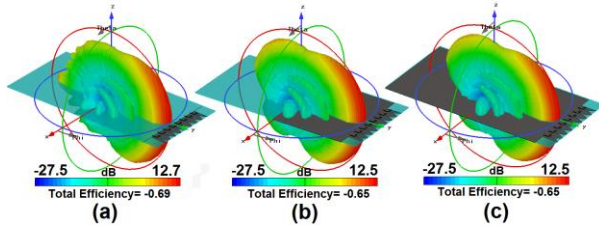

Fig. 18. Radiation characteristics of the 5G mobile-phone antenna (at 0°) for different length of the ground plane: (a) full, (b) half, and (c) without PCB-GND.

The handsets for mobile communication systems are practically operated in the vicinity of a human body. Especially, the user's hand is one of the parts that touch the mobile handsets most frequently [19-20]. In general, the user's hand has a negative impact on the antenna performance in terms of efficiency, gain, impedance-matching etc. Changing its position can increase/ decrease the amount of the losses. The impact of user-hand on the performance of the proposed phased array TSA has been studied and Fig. 19 illustrates different placement of the antenna in the presence of the user's hand.
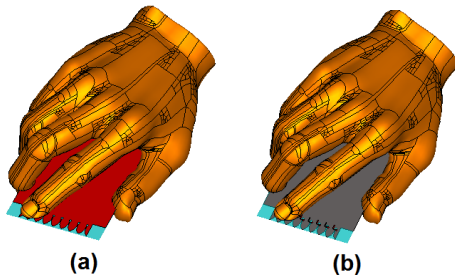

Fig. 19. Different placement of the antenna in the vicinity of user's hand: (a) bottom and (b) top positions.

Table 2 summarizes the effect of user's hand on the properties of the proposed phased array TSA. The total losses of antenna parameters in terms of realized gain, radiation efficiency, and total efficiency are about 3 dB, 15%, and 25%, respectively.

Table 2: Total losses of the antenna parameters

Antenna Parameters	Position (a)	Position (b)
Radiation efficiency	10~25%	10~20%
Total efficiency	20~35%	15~35%
Realized gain	0.5~2.5 dB	1~2 dB

Figure 20 shows the 3D radiation beams of the antenna patterns in the vicinity of user's hand for different scanning angles at different positions. As illustrated, the antenna has a good beam steering function with acceptable gain levels at different scanning angles.

In addition, the S_{nn} characteristics of the designed 5G mobile-phone antenna in the presence of the user's hand is illustrated in Fig. 21. As can be observed, the antenna has good impedance matching with less than 0.4 GHz frequency-shifting in the operation band of the designed array in free space.
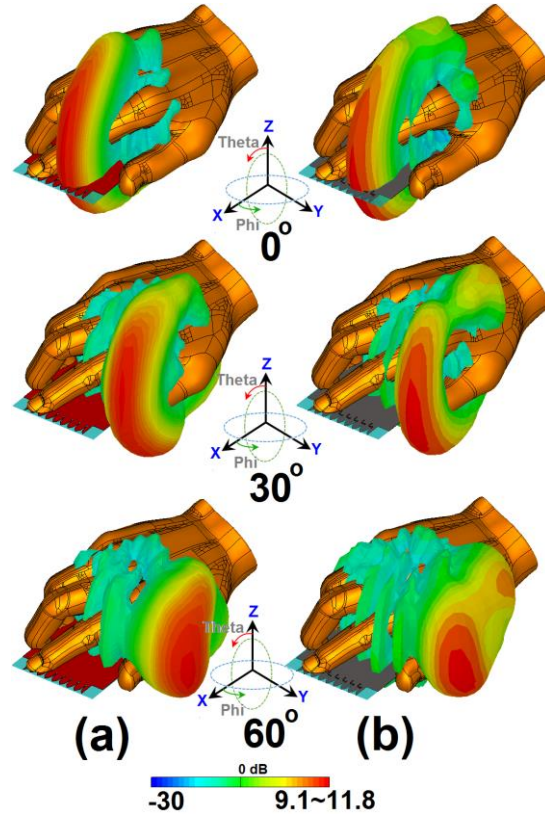

Fig. 20. Radiation beams at different scanning angles for: (a) bottom position and (b) top position.
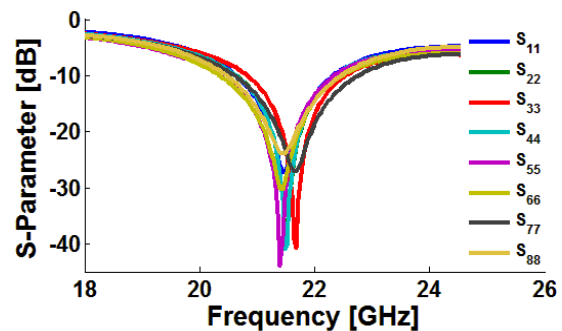

Fig. 21. Snn characteristics of the antenna in the presence of the user-hand (S11 to S88).

The proposed antenna's specification absorption rate (SAR) is studied in Fig. 22. SAR is the measurement of the energy has absorbed by the human body during transmit the radio frequency electromagnetic field. The human body absorbed the energy that's mean we will lose some energy the second problem that's mean will affect the human body badly [21-24]. The SAR is described by the following equation:

$$SAR = \int \frac{\sigma(r)|E(r)|^2}{\rho(r)} dr. \quad (9)$$

As illustrated in Fig. 22, the antenna has sufficient SAR values. It should be noted the distance between 5G antenna PCB and human-hand in z-axis is less than 10 mm. As can be seen, due to close distance of the designed phased array with the head in top location, there is a difference between the SAR values of the top and bottom locations which it was predictable.
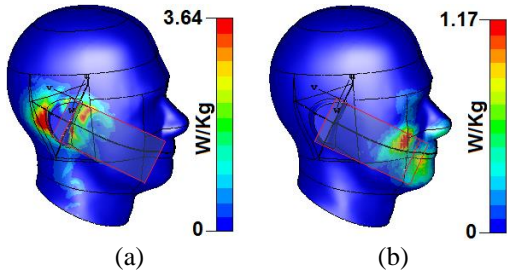

(a) (b)

Fig. 22. Analysis specific absorption rates of the proposed 5G antenna at 22 GHz: (a) top location and (b) bottom location.

Figure 23 depicts the 3D-directional radiation beams of the proposed 5G phased array antenna in the presence of the human-hand (top location) at different scanning angles. As seen, the antenna has good beam-steering characteristics with good gain values at different angles.
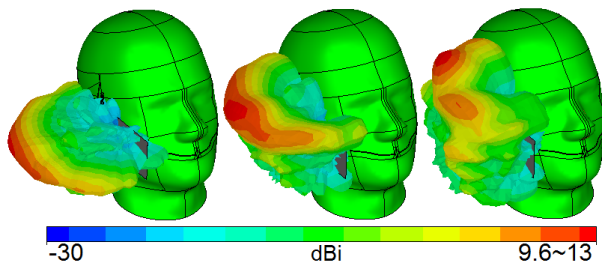

Fig. 23. Radiation beams of the 5G antenna at different angle in the presence of the human-head.

V. PLANAR PHASED ARRAY TSA DESIGN FOR 5G CHANNEL MEASUREMENTS

Figure 24 displays the 3D view of the planar phased array TSA. 64-elements of 22 GHz TSAs with hockey-stick balun Feeds have been used to form the proposed planar array design. On the other hand, the proposed planar array have been designed using eight rows of the proposed linear phased array described in Section III. The designed planar phased array antenna has a compact size of $W_X \times L_X$.
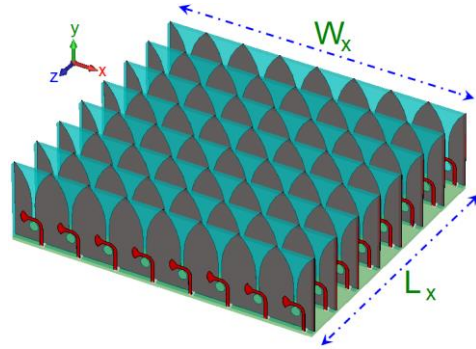

Fig. 24. 3D view of the designed 8×8 planar phased array TSA.

The proposed planar phased array antenna is operating in the same operation band of the single element TSA (frequency range from 21 to 23 GHz). It has compact-size, high-gain, sufficient-efficiency and beam-steering properties. The designed planar array could be used for 5G base station or channel measurement applications [25].

The 3D directional radiation beams of the proposed antenna with directivity values at different angles are shown in Fig. 25. It can be seen that the antenna has a good beam steering characteristic with high-level realized gains. The planar phased array design has more than 21 dB realized gain when its beam is tilted to 0 degree.
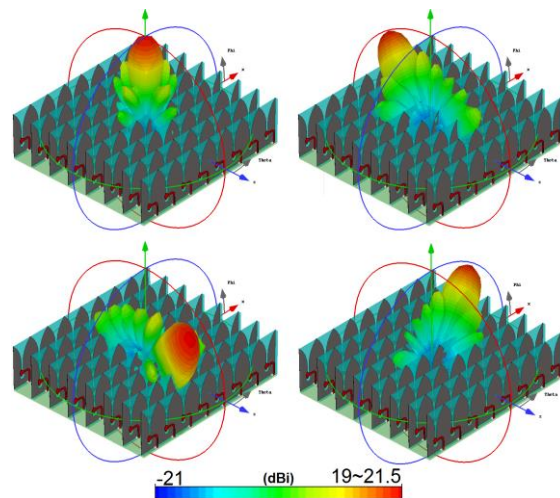

Fig. 25. 3D beams of the proposed phased array at different angles.

VI. CONCLUSION

Low-profile TSA arrays for 5G channel measurement applications are designed and investigated in this study. The antenna elements are designed to work at 22 GHz which is one of the candidate bands for the future communication systems and have a 2 GHz bandwidth. Eight TSA elements formed a linear phased array in the top portion of the mobile-phone PCB. For the deigned 5G mobile-phone antenna, fundamental radiation properties and also user's hand and head impact are studied. The designed array features high-gain/high-efficiency, compact-size good and beam-steering characteristic. In addition, using 8×8 elements of the single element 22 GHz TSA, a planar phased array with high-gain property is designed and its characteristics are investigated. Based on the obtained result, the TSA element, its linear and planar arrays are promising for 5G applications.

REFERENCES

[1] A. Osseiran, et al., "Scenarios for 5G mobile and wireless communications: The vision of the METIS project," *IEEE Commun. Mag.*, vol. 52, pp. 26-35, 2014.

[2] T. S. Rappaport, et al., "Millimeter wave mobile communications for 5G cellular: It will work!," *IEEE Access*, vol. 1, pp. 335-349, 2013.

[3] P. Gupta, "Evolvement of mobile generations: 1G to 5G," *International Journal for Technological Research in Engineering*, vol. 1, pp. 152-157, 2013.

[4] W. Roh, et al., "Millimeter-wave beamforming as an enabling technology for 5G cellular communications: Theoretical feasibility and prototype results," *IEEE Commun. Mag.*, vol. 52, pp. 106-113, 2014.

[5] N. Ojaroudiparchin, M. Shen, and G. F. Pedersen, "A compact design of planar array antenna with fractal elements for future generation applications," *Applied Computational Electromagnetics Society (ACES) Journal*, vol. 31, pp. 789-796, 2016.

[6] K. S. Yngvesson, T. L. Korzeniowski, Y. S. Kim, E. L. Kollberg, and J. F. Johansson, "The tapered slot antema—A new integrated element for MM wave applications," *IEEE Trans. Microw. Theory Tech.*, vol. 37, pp. 365-374, 1989.

[7] A. Kedar and K. S. Beenamole, "Widebeam tapered slot antenna for wide angle scanning phased array antenna," *Progress in Electromagnetics Research*, vo1. 27, pp. 235-251, 2011.

[8] L. S. Locke, J. Bornemann, and S. Claude, "Substrate integrated waveguide-fed tapered slot antenna with smooth performance characteristics over an ultra-wide bandwidth," *Applied Computational Electromagnetics Society (ACES) Journal*, vol. 28, pp. 454-462, 2013.

[9] S. A. Elechi and B. A. Lail, "Design of a high directivity dual tapered slotline antenna," *27th Annual Review of Progress in Applied Computational Electromagnetics*, pp. 839-842, Williamsburg, Virginia, USA, 2011.

[10] W. Hong, K. Baek, Y. Lee, and Y. G. Kim, "Design and analysis of a low-profile 28 GHz beam steering antenna solution for future 5G cellular applications," *IEEE International Microwave Symposium*, Tampa Bay, Florida, June 1-6, 2014.

[11] N. Amitay, V. Galindo, and C. P. Wu, *Theory and Analysis of Phased Array Antennas*. Wiley Interscience, 1972.

[12] W. O. Coburnand and A. I. Zaghloul, "Numerical analysis of stacked tapered slot antennas," *28th Annual Review of Progress in Applied Computational Electromagnetics*, pp. 112-117, Columbus, Ohio, April 10-14, 2012.

[13] J. R. Jamesn and P. S. Hall, *Handbook of Microstrip Antennas*. Peter Peregrinus Ltd., London, 1989.

[14] *CST Microwave Studio.* ver. 2014, CST, Framingham, MA, USA, 2014.

[15] R. C. Hansen, *Phased Array Antennas*, John Wiley & Sons, Inc., New York, 2009.

[16] A. Farahbakhsh, G. Moradi, and S. Mohanna, "Reduction of mutual coupling in microstrip array antenna using polygonal defected ground structure," *Applied Computational Electromagnetics Society (ACES) Journal*, vol. 26, pp. 334-339, 2011.

[17] HMC933LP4E, "*Analog Phase Shifter,*" Hittite Microwave Company.

[18] W. Hong, et al., "mmWave phased-array with hemispheric coverage for5th generation cellular handsets," EuCAP, pp. 714-716, 2014.

[19] N. Ojaroudiparchin, M. Shen, and G. F. Pedersen, "Design of Vivaldi antenna array with end-fire beam steering function for 5G mobile terminals," *Telecommunications Forum (TELFOR 2015)*, Serbia, November 2015.

[20] K. Zhao, Z. Ting, and S. He, "Human exposure to mmwave phased array antennas in mobile terminalfor 5G mobile system," *IEEE Vehicular Technology Conference (VTC Spring)*, Glasgow, pp. 1-2, 2015.

[21] J. Moustafa, N. J. McEwan, R. A. Abd-Alhameed, and P. S. Excell, "Low SAR phased antenna array for mobile handsets," *Applied Computational Electromagnetics Society (ACES) Journal*, vol. 21, pp. 196-205, 2006.

[22] I. B. Bonev, O. Franek, and G. F. Pedersen, "Impact of the hand on the specific absorption rate in the head," *Applied Computational Electromagnetics Society (ACES) Journal*, vol. 29, pp. 470-

477, 2014.

[23] M. R. I. Faruque, M. T. Islam, and N. Misran, "Evaluation of EM absorption in human head with metamaterial attachment," *Applied Computational Electromagnetics Society (ACES) Journal*, pp. 1097-1107, vol. 25, 2010.

[24] M. Fallah, A. A. Heydari, A. R. Mallahzadeh, and F. H. Kashani, "Design and SAR reduction of the vest antenna using metamaterial for broadband applications," *Applied Computational Electromagnetics Society (ACES) Journal*, vol. 26, pp. 141-155, 2011.

[25] N. Ojaroudiparchin, M. Shen, and G. F. Pedersen, "8×8 planar phased array antenna with high efficiency and insensitivity properties for 5G mobile base stations," *EuCAP 2016*, Switzerland, 2016.

Naser Ojaroudi Parchin was born on 1986 in Iran. He received M.Sc. degree in Telecommunication Engineering from Shahid Rajaee University (SRTTU), Tehran, Iran in 2013. His research interests include multi-band/UWB antennas, MIMO antennas, Fabry resonators, Fractal antennas, mm-Wave phased array 5G antennas, band-stop/band-pass microwave filters, and reconfigurable structure.
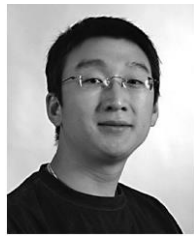
Ming Shen received the Master and Ph.D. degrees in Electrical Engineering from the University of Chinese Academy of Sciences, China in 2005, and from Aalborg University, Denmark in 2010, respectively. Since 2007, he has been with the Department of Electronic Systems, Aalborg University, where he is currently an Assistant Professor. He is the author of more than 30 technical papers and book chapters. His current research interests include: energy harvesting and battery-less low power circuits and systems, 5G mm-Wave circuits and antennas, remote patient monitoring, and wireless power transfer technologies.

Gert Frølund Pedersen received the B.Sc. E. E. degree, with honor, in Electrical Engineering from College of Technology in Dublin, Ireland in 1991, and the M.Sc. E. E. degree and Ph.D. from Aalborg University in 1993 and 2003. He has been with Aalborg University since 1993 where he is a Full Professor heading the Antenna, Propagation and Networking LAB with 36 researchers. Further he is also the Head of the doctoral school on wireless communication with some 100 Ph.D. students enrolled. His research has focused on radio communication for mobile terminals especially small Antennas, Diversity systems, Propagation and Biological effects and he has published more than 175 peer-reviewed papers and holds 28 patents. He has also worked as Consultant for developments of more than 100 antennas for mobile terminals including the first internal antenna for mobile phones in 1994 with lowest SAR, first internal triple-band antenna in1998 with low SAR and high TRP and TIS, and lately various multi antenna systems rated as the most efficient on the market. He has worked most of the time with joint university and industry projects and have received more than 12 M$ in direct research funding. Latest he is the project leader of the SAFE project with a total budget of 8 M$ investigating tunable front end including tunable antennas for the future multiband mobile phones. He has been one of the pioneers in establishing Over-The-Air (OTA) measurement systems. The measurement technique is now well established for mobile terminals with single antennas and he was chairing the various COST groups (swg2.2 of COST 259, 273, 2100 and now ICT1004) with liaison to 3GPP for over-the air test of MIMO terminals.